Finding unprecedentedly low-thermal-conductivity half-Heusler semiconductors via high-throughput materials modeling

Jesús Carrete, Wu Li, and Natalio Mingo*
CEA-Grenoble, 17 Rue des Martyrs, Grenoble 38054, France

Shidong Wang and Stefano Curtarolo†
Center for Materials Genomics, Materials Science, Electrical Engineering, Physics and Chemistry, Duke University, Durham, North Carolina 27708, USA

arXiv:1401.2439v2 [cond-mat.mtrl-sci] 21 Feb 2014

The lattice thermal conductivity (κ_ω) is a key property for many potential applications of compounds. Discovery of materials with very low or high κ_ω remains an experimental challenge due to high costs and time-consuming synthesis procedures. High-throughput computational pre-screening is a valuable approach for significantly reducing the set of candidate compounds. In this article, we introduce efficient methods for reliably estimating the bulk κ_ω for a large number of compounds. The algorithms are based on a combination of machine-learning algorithms, physical insights, and automatic *ab-initio* calculations. We scanned approximately 79,000 half-Heusler entries in the AFLOWLIB.org database. Among the 450 mechanically stable ordered semiconductors identified, we find that κ_ω spans more than two orders of magnitude- a much larger range than that previously thought. κ_ω is lowest for compounds whose elements in equivalent positions have large atomic radii. We then perform a thorough screening of thermodynamical stability that allows to reduce the list to 77 systems. We can then provide a quantitative estimate of κ_ω for this selected range of systems. Three semiconductors having $\kappa_\omega < 5\,\mathrm{W\,m^{-1}\,K^{-1}}$ are proposed for further experimental study.

INTRODUCTION

High-throughput (HT) computational materials science is a rapidly expanding area of materials research. It merges a plethora of techniques from a variety of disciplines. These include the kinetics and thermodynamics of materials, solid-state physics, artificial intelligence, computer science, and statistics [1]. The application of HT has recently led to new insights and novel compounds in different fields [2–9]. Despite the importance of thermal transport properties for many crucial technologies, there are to date no high-throughput investigations into lattice thermal conductivity.

Here we seek to address this challenge. We concentrate on the lattice thermal conductivity of half-Heusler compounds, as they have great promise for applications as thermoelectric materials [10–13]. Half-Heusler compounds are ternary solids. Their crystalline structure consists of two atoms (A and B), located in equivalent positions in a rock-salt structure. A third atom (X) sits in an inequivalent position, filling half of the octahedrally coordinated sites (Fig. 1a).

Experimental studies have reported the thermoelectric figure of merit for a small set of these systems and their alloys [14–18]. Theoretical electronic characterizations have been performed for 36 candidates [19]. It has been speculated that their high thermal conductivity, close to $10\,\mathrm{W\,m^{-1}\,K^{-1}}$, could limit thermoelectric performance [20, 21]. At room temperature, the lattice thermal conductivity κ_ω represents the largest contribution to the total conductivity.

Promising thermoelectric figures of merit have been reported both for n-type (1.5 at 700 K [22]) and for p-type (0.8 at 1000 K [17]) half-Heuslers. Such values are comparable to the best thermoelectric materials proposed thus far [23]. Those values, however, were not found in ordered half-Heuslers; but rather in alloyed or nanostructured systems. Furthermore, finding ordered compounds with very low κ_ω is advantageous, as their electronic mobilities are expected to be higher than in alloys. In addition, alloying the already low-κ_ω ordered compounds would lower κ_ω even further.

The pool of candidate compounds analyzed in this article is larger than in previous investigations. All possible half-Heusler compounds from all combinations of non-radioactive elements in the periodic table are considered, as included in the AFLOWLIB.org consortium repository [24] (Fig. 1b). The formation enthalpies of the fully relaxed structures are obtained through density functional theory within the AFLOW high-throughput framework [25].

From a total of 79,057 entries, those with positive formation enthalpies are removed. When several half-Heuslers are related by permutations of elements, only the lowest-enthalpy configurations are considered. Finally, zero-gap compounds are removed from the list. For the surviving subset of 995 compounds, the second-order force constants are characterized with full phonon dispersion curves. This allows further reduction of the set to a total of 450 mechanically stable semiconductors. Although these requirements do not guarantee global thermodynamical stability, metastable compounds with long lifetimes have been synthesized and used [26]. Hence, their inclusion should not be disregarded *a priori*.

For the 450 resulting stable half-Heuslers, we compute a large set of structural, electronic and harmonic proper-

ties. In principle, one could directly compute κ_ω for all the compounds. The computational requirements for this approach would be prohibitive. To solve this issue, our strategy is to obtain κ_ω for a smaller subset of systems. We use physical insights and machine learning techniques to predict the remaining values. Cross-validation shows that the approach is reliable for rapidly identifying low-κ_ω compounds.

Once the main factors correlated with a low thermal conductivity are identified for the 450-HH library, we use the thermodynamical information in the AFLOWLIB.org database to test the stability of these HHs against more than 110,000 phases. All competing ternary compounds from the Inorganic Crystal Structure Database (ICSD) [27] and all binaries in that database sharing two elements with each HH are included. The final list of thermodynamically stable compounds contains 77 entries. For these we devise and implement a novel approach to compute the lattice thermal conductivity. Our accuracy is better than 50% of the exact calculation, and has a much lower computational cost. This allows to provide estimates of κ_ω that can be compared with experiment for 77 thermodynamically stable compounds.

PREDICTING BULK LATTICE THERMAL CONDUCTIVITIES

The general expression for κ_ω at temperature T is [28]:

$$\kappa_\omega = \frac{1}{k_B T^2 V} \sum_\lambda n_0 \left(n_0+1\right) |v_\lambda^{(z)}|^2 \hbar^2 \omega_\lambda^2 \tau_\lambda, \qquad (1)$$

where λ denotes the phonon branch index α and wave vector $\mathbf{q}$, k_B is Boltzmann's constant, n_0 the Bose-Einstein distribution, ω_λ the frequency of phonons, $v_\lambda^{(z)}$ the phonon group velocity in the transport direction z, and τ_λ the relaxation time. The relaxation time is determined by third-order derivatives of the total energy with respect to the atomic displacements of any three atoms i, j, and k in directions a b and c (Φ_{ijk}^{abc}, the anharmonic force constants) in a large supercell [29].

In ordered half-Heuslers the dominant source of scattering is due to three-phonon processes, and we can calculate thermal conductivities with the full *ab-initio* anharmonic characterization [30, 31]. For CoSbZr, one of the most thoroughly studied half-Heuslers, we obtain $\kappa_\omega = 25.0\,\mathrm{W\,m^{-1}\,K^{-1}}$. The value is very close to a previous theoretical estimate ($\sim 22\,\mathrm{W\,m^{-1}\,K^{-1}}$) for monocrystalline CoSbZr [19], and slightly higher than the experimental values [32, 33] (between 15 and $20\,\mathrm{W\,m^{-1}\,K^{-1}}$). Synthesized samples of Refs. [32, 33] may contain microstructures and imperfections not considered in our work. Despite of accuracy, "full *ab-initio* calculations" of κ_ω (Eq. 1) are prohibitive for HT studies, due to the computational requirements of the derivatives giving τ_λ.

In this section, we present two different approaches circumventing the limitation. The first method is based on the empirical observation that the force constants show high degree of transferability between compounds sharing crystal structure [34]. This suggests that a single set of anharmonic force constants could be used to get an estimate of the bulk κ_ω. We call this thermal conductivity calculated with "transferred" forces κ_{transf} (see Table II).

We desired to preserve the choice between equivalent positions for maximizing transferability. Thus, instead of taking the anharmonic force constants of a particular half-Heusler compound, we choose those of Mg_2Si. This compound shares the half-Heusler lattice with sites A and B occupied by Mg atoms. For cross-validation, we also fully compute the anharmonic force constants of 32 half-Heusler systems. These are randomly selected with uniform probability inside the convex hull of Fig. 2a, to ensure a wide variety of harmonic/anharmonic features. Comparison between κ_ω and κ_{transf} indicates that- although the latter has limited quantitative precision- the qualitative agreement is very good; with a Spearman rank correlation coefficient of 0.93. Hence, the descriptor can be effectively used to separate compounds having high or low κ_ω. Note that we chose the Spearman rank correlation [35] instead of the usual Pearson's. The former is invariant under any monotonic transformation of one or both variables, and takes values ± 1 for any strict monotonic (not just linear) dependence.

The second proposed approach is based on a completely different direction: we use "random-forest regression" by leveraging the 32 fully calculated κ_ω as a training set. We can then employ the fitted model to predict the remaining conductivities. We call these predictions κ_{forest} (see Table II). Random forests [36] are a general classification and regression algorithms and the are well adapted to dependent input data. They have already been successfully applied to numerous problems [37, 38], including compound classification [39]. Here, the 32 compounds represent only around 7% of the mechanically stable half-Heuslers. Our input data comprises a large set of descriptor variables, which is expected to correlate with κ_ω (supplementary materials) but is less expensive to obtain. Descriptors include:

- *A priori* chemical information: atomic number and weight, position in the periodic table, atomic radius, Pauling electronegativity [40], and Pettifor's chemical scale χ (Ref. 41).

- General compound information: lattice constant a_{latt}, band gap, formation enthalpy, effective masses of electrons and holes, Born effective charges and dielectric tensor.

- Specific thermal conductivity information: specific heat c_v, spherically-averaged speed of sound c_s, scaled nanograined-limit thermal conductivity $\tilde{\kappa}_{\mathrm{grain}}$ and phase-space volume available for three-phonon scattering processes P_3.

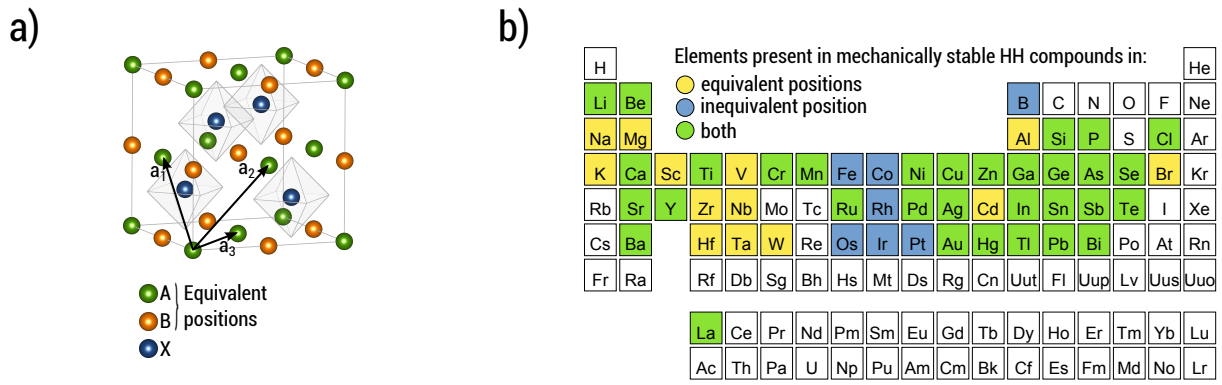

FIG. 1: **(a)** Prototype Half-Heusler structure with primitive vectors and conventional cell. **(b)** Elements considered in this study.

	κ_ω [W m^{-1} K^{-1}]	$\sigma_{\text{forest,CV}}$ [%]		κ_ω [W m^{-1} K^{-1}]	$\sigma_{\text{forest,CV}}$ [%]		κ_ω [W m^{-1} K^{-1}]	$\sigma_{\text{forest,CV}}$ [%]
AgKTe	0.508	42	GeCaZn	2.75	9.6	PtGaTa	32.9	11
BeNaP	4.08	20	GeNaY	8.06	14	PtGeTi	16.9	9.0
BiBaK	2.19	11	InBaSr	0.582	15	PtInNb	16.5	8.2
BiKSr	1.96	6.4	IrPTi	27.4	7.8	RhHfSb	21.8	13
BiLiSr	3.04	10	NiPbTi	109	10	RhNbSi	15.3	11
CoAsZr	24.0	7.4	NiSbSc	19.5	11	RuAsV	23.5	13
CoBiHf	18.6	14	NiSnTi	17.9	9.3	SbCaK	2.70	9.3
CoSbZr	25.0	2.4	NiSnZr	19.6	11	SiCdSr	13.5	19
CoScSe	15.0	13	OsSbTa	26.9	12	SnBaSr	2.01	43
CoSiTa	37.8	7.7	PdAsY	5.48	9.5	TeAgLi	1.52	11
FeNbP	109	4.2	PdSrTe	1.16	19			

TABLE I: Fully calculated thermal conductivities, κ_ω, for 32 compounds. These results are then used as the training set for the random-forest predictions. An estimate of the relative standard deviation of κ_{forest} for each compound in the training set, as obtained using repeated 4-fold cross-validation, is also included. Compounds are always labeled with the element in position X first.

Label	Definition
κ_ω	Lattice contribution to κ from the "full calculation"
κ_{transf}	Approximated κ_ω with anharmonic force constants from Mg_2Si
κ_{forest}	κ_ω obtained from random-forest regression
κ_{anh}	κ_ω obtained with four exact anharmonic force constants and a linear model for the remaining
κ_e	Electronic contribution to κ
$\tilde{\kappa}_{\text{grain}}$	Scaled nanograined-limit κ_ω

TABLE II: Notation for thermal conductivities.

After an exploratory phase, we conclude that a satisfactory fit can be safely achieved using only *a priori* data.

The random-forest method is performed in three steps. First, a large ensemble of decision trees is built by randomly selecting subsets of descriptors and observations. Second, the predictions of all trees are obtained for each data point. Third, the mode (for classification) or the mean (for regression) are taken as the result from the whole ensemble. The algorithm also provides an intrinsic metric to evaluate the importance of each descriptor. This is defined in relation to the effect of randomly permuting the values of that variable on the result [36] (the less resilient upon permutation, the more important).

The prediction of each tree in a random forest can only be a value from the training set, and thus the result of the regression is a weighted average. This average is bounded by the minimum and maximum values within the training data. A small set is unlikely to contain elements having extreme values. Hence, our random-forest regression is expected to have a marked centralizing effect, yielding values tightly grouped around their mean. The frequency densities of both κ_{transf} and this new κ_{forest} are displayed in Fig. 2b. The latter avoids extreme predictions with non-physical magnitudes, a result of the aforementioned centralizing effect.

In this sense, machine-learning algorithms outperform crude extrapolations such as those behind κ_{transf}. Additionally, κ_{forest} has the advantage that its predictions can be refined with controlled accuracy by changing the size of the training set. Even so, the Spearman rank corre-

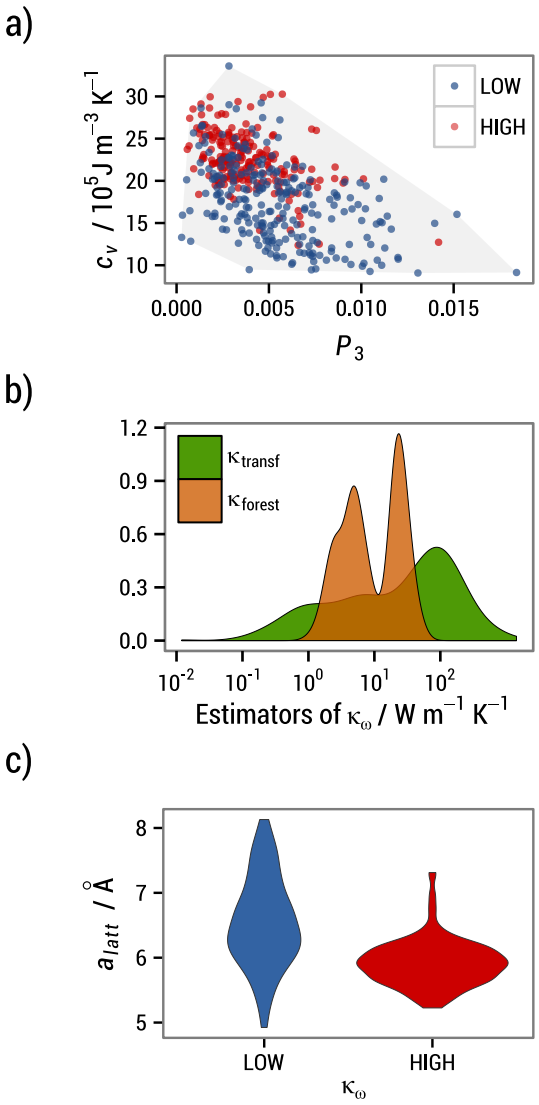

FIG. 2: **(a)** Joint scatter plot of c_v at 300 K and P_3 colored according to our low/high-κ_ω classification based on κ_{forest} (see text); the convex hull of the point set is also included for guidance. **(b)** Frequency densities of the estimators of thermal conductivity at 300 K κ_{transf} and κ_{forest} as defined in the text. **(c)** "Violin plot" showing the distribution of a_{latt} within the low- and high-κ_ω classes.

lation coefficient between κ_{transf} and κ_{forest} is still 0.66, corroborating the validity of the analysis based on κ_{forest}. Furthermore, we find that κ_{forest} is strongly correlated with physical descriptors like c_v, $\tilde{\kappa}_{\text{grain}}$, and P_3. This confirms our earlier speculation about these methods.

An important concern when training a machine-learning model is whether the training set is diverse or representative enough to justify extrapolating the model to the remaining elements. The values of κ_ω needed for direct validation of the predicted κ_{forest} are unavailable. Thus, we resort to a repeated 4-fold cross-validation among the data points in the training set to obtain an estimate of the out-of-sample error. More specifically, we evenly split our training set into 4 subsets. Then, we obtain a random-forest prediction for the HHs in each of the subsets by using only the remaining 75% of compounds as the new training set. We repeat the process 10 times for different divisions of the data, and compute the standard deviation of these predictions. The results are included in Table. I. These estimates support the notion that the model behind κ_{forest} is reasonably insensitive to our choice of training sets. For each cross-validation, we compute the Spearman rank correlation coefficient between the out-of-sample random-forest results for the 32 training compounds and their κ_ω. The median value of these Spearman rank correlation coefficients is 0.74, corroborating κ_{forest} as a reliable tool for predicting compounds' ordering.

The ordering predicted by descriptor κ_{forest} is strongly correlated with that of κ_ω. This allows to pinpoint the main factors determining high or low thermal conductivities. The bimodal shape of the distribution in Fig. 2b suggests that two groups of half-Heuslers can be identified, with thermal conductivities spread around two different values. A robust version of the "k-means" algorithm [42] is employed to optimally place the medians of the low- and high-thermal-conductivity classes at 4.50 and 23.1 W m^{-1} K^{-1}, respectively. By analyzing the importance of variables in the classification, we identify a low Pettifor scale χ_X and a large average Pauling electronegativity $\bar{e}_{AB}$ as the most critical descriptors for low conductivity (supplementary materials).

Given the underlying correlations, many different choices can be used for the classification. A trend can even be suggested on the grounds of atomic radii by following a chain of correlations: if the two elements in equivalent positions are chosen so that their average radius is larger than 150 pm, then the probability of the compound being in the low-κ_ω class is 84%. Physically, this follows from the fact that κ_ω is highly correlated with the specific heat c_v (Fig. 2a). The latter is strongly negatively correlated with the lattice parameter a_{latt}: the larger a_{latt} the lower c_v [57].

In addition, a_{latt} correlates well with the sum of the atomic radii of the three elements, quantities known *a priori*. The atomic radii of the species in positions X concentrate around the average value. This leads to an accurate prediction of a_{latt} by using only the average atomic radius of atoms in positions A and B, $\bar{r}_{AB}$. A large $\bar{r}_{AB}$ causes a large lattice constant, small specific heat, and finally, low thermal conductivity. Alternatively, the lattice parameter can be used as a good discriminant: panel (c) in Fig. 2 is a "violin plot" illustrating the distribution of a_{latt} in the classes of half-Heuslers with low and high thermal conductivities. Also, as it can be seen in Fig. 2a our choice of easily computable descriptors such as c_v and P_3 is supported by the result of this classification.

Our calculations are for the true bulk lattice thermal conductivity. They are unrelated to the minimum value proposed by other authors [43, 44]. Nevertheless, some of the κ_ω obtained directly seem ultra-low. They are

even lower than $\sim 0.70\,\mathrm{W\,m^{-1}\,K^{-1}}$, as reported in literature for $AgSbTe_2$ and $AgBiSe_2$ [45], and described as close to the achievable minimum. However, the minimum depends on the compound's structure. Even within the most stringent hypothesis of the shortest possible mean free path equal to interatomic spacing, the lowest found κ_ω is much higher than the theoretical minimum. Therefore, none of our predicted values violates the minimum lattice thermal conductivity. Note also that, once the goal of reducing the κ_ω under $\lesssim 1\,\mathrm{W\,m^{-1}\,K^{-1}}$ is achieved, its precise value loses relevancy as it is overtaken by the contribution of charge carriers, κ_e.

SCREENING FOR THERMODYNAMICAL STABILITY

The ingredients of κ_ω for bulk ordered semiconductors depend only on a semilocal characterization of the potential energy surface around the equilibrium configuration. Hence, mechanical stability is sufficient to permit the calculation of the lattice thermal conductivity of a HH. For the analysis performed in the previous section, having the set of 450 mechanically stable HHs reduced and biased by external considerations such as thermodynamical stability would be detrimental to the performance of machine-learning techniques.

On the other hand, in order to propose particular candidates for experimentation we must maximize the probability that they can be obtained in the laboratory. To this end, we obtain the ternary phase diagrams for each of the 450 mechanically stable HHs. This involves taking into account the formation enthalpies of a large number of possible competing phases. These include but are not limited to all relevant binary and ternary compounds in the ICSD [27]. More specifically, all the elemental compounds, 109, 136 binary structures and 4, 363 ternary phases were considered. Many of these phases were already present in AFLOWLIB.org; others were computed specifically for this work. The total number of DFT calculations necessary to obtain the results presented here exceeds 300, 000. Our thermodynamic analysis reveals that 79 of the 450 HHs are thermodynamically stable. Spin-polarized calculations reveal that two of the 79 have semimetallic ground states. Then, only the remaining 77 compounds are further considered. The ternary phase diagrams of the final 77 systems are included in the supplementary materials.

76 of the 77 predicted stable compounds satisfy the octet or expanded octet rules by virtue of having 8 or 18 valence electrons per unit cell, respectively. We compared these numbers with the frequency distribution of valence electron counts in the initial 79, 057-HH library. We conclude that the conditional probabilities of compounds having 8 or 18 valence electrons per unit cell being stable are 1.2% and 3.8%, respectively. While still small, the conditional likelihood of a compound satisfying one of these rules making it through all the filtering steps is much higher than the 0.1% *a priori* probability. Fig. 3 shows the distribution of the valence during the reduction of prototypes' list. Only the compound LaClSe (valence=16) does not seem to follow the rule.

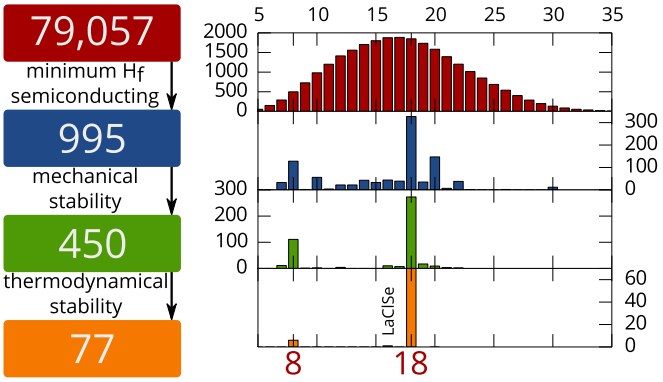

FIG. 3: Number of compounds during the screening (left) and evolution of the valence per unit cell distribution (right). Of the final 77 compounds, only LaClSe (valence=16) does not seem to follow the 8/18 octet rule.

Even among the reduced list, κ_{forest} still spans more than one order of magnitude, its extreme values being 2.33 and $40.3\,\mathrm{W\,m^{-1}\,K^{-1}}$, reinforcing our previous conclusions.

A DESCRIPTOR WITH QUANTITATIVE POWER

Neither of the two descriptors of κ_ω presented so far contains any information about the anharmonic interatomic force constants (IFCs) of each compound. On one hand, the last round of thermodynamical screening puts the number of surviving HHs within the limits of what can be realistically considered for anharmonic calculations. On the other, the qualitative success of κ_{transf} shows that a detailed anharmonic description is not required. To enhance our estimates of the thermal conductivity of stable half-Heuslers, in this section we present a new machine-learning descriptor of κ_ω that integrates only the crucial pieces of the anharmonic properties of the solid. This aids in achieving quantitative accuracy with a much lower computational cost than the full calculation.

Crystallographic symmetries and the equality of mixed partials impose linear constraints on the anharmonic IFCs. With the parameters described in the "Methods" section below and those constraints, we are left with 737 independent anharmonic IFCs per compound. However, many elements of this set are correlated among them, and others are too small to have a decisive role in the value of κ_ω. To quantify these assertions, we perform principal component analysis [46] on the third-order IFCs for the 32 compounds in Table. I.

We find that the first four components account for $\sim$ 99% of the variance in the set. From the results we

can extract an expression for each of the 737 IFCs as a linear combination of those components. Then we perform a multivariable multiple linear regression of the four components on four large and weakly correlated IFCs. By combining the two results, we arrive at a linear model for the whole set of anharmonic IFCs in terms of four parameters that can be obtained with 16 DFT calculations per compound. We use the term κ_ω to describe the third-order IFCs thus reconstructed, and $\kappa_{\rm anh}$ for the second-order IFCs for each compound.

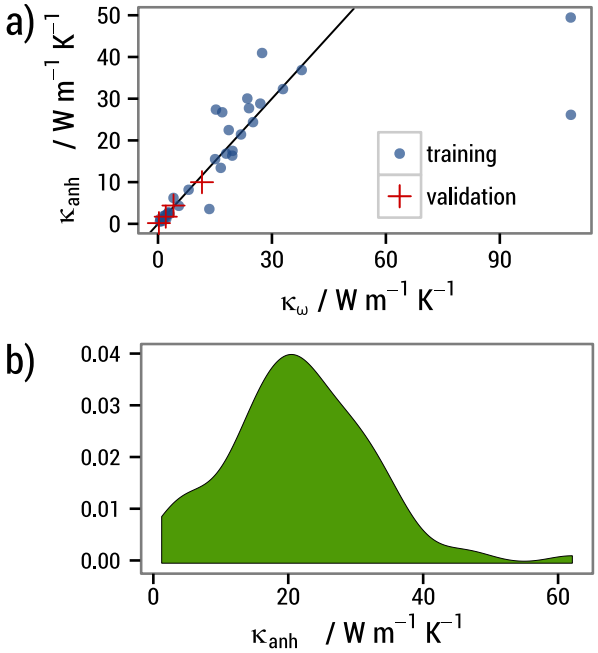

FIG. 4: **(a)** Comparison of $\kappa_{\rm anh}$ with the exact κ_ω for the 32 compounds in the training set and the three compounds used for validation. **(b)** Distribution of $\kappa_{\rm anh}$ over the 77 thermodynamically stable HHs.

The blue circles in Fig. 4a show a comparison between $\kappa_{\rm anh}$ and the exact κ_ω for the 32 compounds in the training set. With two exceptions (compounds with comparatively very high thermal conductivities) this new descriptor yields excellent quantitative estimates of κ_ω. Moreover, 4-fold cross-validation shows that it is insensitive to the particular choice of training set. As a final test, we perform full thermal conductivity calculations for four compounds selected at random from those outside the training set: AgBaSb, AgNaTe, InCdY and TlLaMg. The results are depicted as red crosses in Fig. 4a. This shows that the quality of the prediction is as good as for the 32 training compounds.

The distribution of $\kappa_{\rm anh}$ over the 77 thermodynamically stable HHs (Fig. 4b) confirms the presence in the sample of compounds with thermal conductivities much lower that the $10-20\,{\rm W\,m^{-1}\,K^{-1}}$. This is characteristic of experimentally measured HHs. The values of $\kappa_{\rm anh}$ for the 77 stable HHs is listed in Table III. Notably, the subset of 10 thermodynamically stable half-Heuslers for which κ_ω was directly computed already contains BiBaK, with $\kappa_\omega = 2.20\,{\rm W\,m^{-1}\,K^{-1}}$. Outside of the training sample, the lowest $\kappa_{\rm anh}$ values are 1.72, 2.84 and 3.49 for PtLaSb, RhLaTe and SbNaSr, respectively.

CONCLUSIONS

In this article, we have presented three computational methods for estimating the bulk κ_ω of a large library of half-Heusler compounds. We surmount the formidable task of full *ab-initio* characterization. We find that κ_ω is spread over more than two orders of magnitude over mechanically stable half-Heuslers. This is a much broader range than that suggested by limited experimental available data. By using a set of descriptors and random-forest regression, we have built and tested an effective classification model. We found that compounds are most likely to have low thermal conductivity if the average atomic radius of the atoms in structural positions A and B is large. This also correlates with large lattice parameters and low specific heats.

Extensive thermodynamical calculations allow to remove from the list compounds with more stable competing phases. We employ our third method, with better quantitative accuracy and higher computational cost, to perform a finer analysis of the distribution of κ_ω over the reduced library. We conclude ordered half-Heusler compounds with $\kappa_\omega \lesssim 3\,{\rm W\,m^{-1}\,K^{-1}}$ value (a factor of three below the best scenarios for ordered compounds, and comparable to alloyed systems) very likely exist. The results corroborate the competitiveness of machine-learning methods in accelerated material design [1].

METHODS

AFLOWLIB library of half-Heusler systems. The 79,057 half-Heusler systems are calculated with the high-throughput framework AFLOW [4, 25, 47, 48] based on *ab-initio* calculations of the energies by the VASP software [49] with projector augmented waves (PAW) pseudopotentials [50], and Perdew, Burke and Ernzerhof exchange-correlation functionals [51]. The AFLOWLIB energies are calculated at zero temperature and pressure, with spin polarization and without zero-point motion or lattice vibrations. All crystal structures are fully relaxed (cell volume and shape and the basis atom coordinates inside the cell). Numerical convergence to about $1\,{\rm meV\,atom^{-1}}$ is ensured by a high energy cutoff (30% higher than the highest energy cutoff for the pseudopotentials of the components) and by the dense 6,000 **k**-points per reciprocal atom Monkhorst-Pack meshes [52].

Interatomic force constants. $3\times3\times3$ supercells are used in second-order IFC calculations. The Phonopy [53] package is used to generate a minimal set of atomic displacements by harnessing the point and translational

	κ_{anh} [W m^{-1} K^{-1}]		κ_{anh} [W m^{-1} K^{-1}]		κ_{anh} [W m^{-1} K^{-1}]		κ_{anh} [W m^{-1} K^{-1}]
AuAlHf	16.7	FeAsNb	47.6	NiBiY	10.6	PtLaSb	1.72
BLiSi	62.1	FeAsTa	32.9	NiGaNb	22.9	RhAsTi	33.1
BiBaK	1.24	FeGeW	32.8	NiGeHf	19.6	RhAsZr	27.1
CoAsHf	20.0	FeNbSb	29.1	NiGeTi	25.3	RhBiHf	12.8
CoAsTi	37.1	FeSbTa	31.2	NiGeZr	21.1	RhBiTi	13.0
CoAsZr	27.7	FeSbV	24.1	NiHfSn	19.5	RhBiZr	13.0
CoBiHf	22.5	FeTeTi	26.2	NiPbZr	15.2	RhLaTe	2.84
CoBiTi	27.1	GeAlLi	16.5	NiSnTi	16.8	RhNbSn	15.7
CoBiZr	17.8	IrAsTi	30.1	NiSnZr	17.5	RhSnTa	20.3
CoGeNb	36.2	IrAsZr	17.4	OsNbSb	24.8	RuAsNb	43.7
CoGeTa	27.2	IrBiZr	12.8	OsSbTa	28.8	RuAsTa	33.4
CoGeV	29.1	IrGeNb	33.0	PCdNa	6.05	RuNbSb	22.7
CoHfSb	21.9	IrGeTa	37.2	PNaSr	6.30	RuSbTa	20.9
CoNbSi	30.1	IrGeV	30.0	PdBiSc	9.95	RuTeZr	21.3
CoNbSn	20.7	IrHfSb	24.7	PdGeZr	18.2	SbNaSr	3.49
CoSbTi	23.3	IrNbSn	19.8	PdHfSn	15.1	SiAlLi	20.9
CoSbZr	24.4	IrSnTa	22.1	PdPbZr	10.3	ZnLiSb	6.44
CoSiTa	36.9	LaClSe	5.71	PtGaTa	32.3		
CoSnTa	22.7	NiAsSc	17.5	PtGeTi	26.7		
CoSnV	19.8	NiBiSc	14.3	PtGeZr	15.9		

TABLE III: The values of $\kappa_{\rm anh}$ for the 77 thermodynamically stable half-Heusler compounds.

symmetries of the crystal structure, and custom software was developed in order to do the same in anharmonic IFC calculations. For those, $4\times4\times4$ supercells are generated and a cutoff radius of $0.85a_{\rm latt}$ is imposed on the interactions. $2\times2\times2$ and $3\times3\times3$ Monkhorst-Pack **k**-point grids are employed, and spin polarization excluded to improve speed.

Solution of the Boltzmann transport equation. Our self-consistent iterative approach is described in detail in Ref. 30. Both three-phonon processes and the natural isotopic distribution of each element are taken into account as sources of scattering. A Gaussian smearing scheme with adaptive breadth [31] is chosen for integrations in the Brillouin zone. When using anharmonic IFCs from Mg_2Si to approximate κ_ω for all materials, the solution to the Boltzmann transport equation failed to converge for 5 compounds, which are consequently excluded from the associated analysis.

Regression and classification. The R statistical computing environment [54] is chosen for all statistical analyses. Random-forest models are used as implemented in the "randomForest" package [55]. As a check, all regressions and classifications are repeated using a generalized boosted tree algorithm [56]; in all cases the results are found to be in good agreement with those afforded by random forests.

ACKNOWLEDGMENTS

The authors thank Prof. D. Broido and Dr. L. Lindsay for providing us with a set of anharmonic force constants for Mg_2Si, and Dr. A. Stelling, Dr. O. Levy, Prof. S. Sanvito, Prof. M. Buongiorno Nardelli, and Prof. M. Fornari for useful comments. This work is partially supported by the French "Carnot" project SIEVE, by DOD-ONR (N00014-13-1-0635, N00014-11-1-0136, N00014-09-1-0921) and by the Duke University—Center for Materials Genomics.

* Electronic address: natalio.mingo@cea.fr
† Electronic address: stefano@duke.edu

[1] S. Curtarolo, G. L. W. Hart, M. Buongiorno Nardelli, N. Mingo, S. Sanvito, and O. Levy, *The high-throughput highway to computational materials design*, Nature Mater. **12**, 191–201 (2013).
[2] J. Greeley, T. F. Jaramillo, J. Bonde, I. Chorkendorff, and J. K. Nørskov, *Computational high-throughput screening of electrocatalytic materials for hydrogen evolution*, Nature Mater. **5**, 909–913 (2006).
[3] G. Ceder, G. Hauthier, A. Jain, and S. P. Ong, *Recharging lithium battery research with first-principles methods*, MRS Bull. **36**, 185–191 (2011).
[4] S. Wang, Z. Wang, W. Setyawan, N. Mingo, and S. Curtarolo, *Assessing the thermoelectric properties of sintered compounds via high-throughput ab-initio calculations*, Phys. Rev. X **1**, 021012 (2011).
[5] I. E. Castelli, T. Olsen, S. Datta, D. D. Landis, S. Dahl, K. S. Thygesen, and K. W. Jacobsen, *Computational screening of perovskite metal oxides for optimal solar light capture*, Energy & Environmental Science **5**, 5814–5819 (2012).
[6] L. Yu and A. Zunger, *Identification of Potential Photovoltaic Absorbers Based on First-Principles Spectroscopic Screening of Materials*, Phys. Rev. Lett. **108**, 068701 (2012).
[7] K. Yang, W. Setyawan, S. Wang, M. Buongiorno Nardelli,

and S. Curtarolo, *A search model for topological insulators with high-throughput robustness descriptors*, Nature Mater. **11**, 614–619 (2012).

[8] G. Ceder and K. Persson, *How Supercomputers Will Yield a Golden Age of Materials Science*, Scientific American (Dec 2013).

[9] G. L. W. Hart, S. Curtarolo, T. B. Massalski, and O. Levy, *Comprehensive Search for New Phases and Compounds in Binary Alloy Systems Based on Platinum-Group Metals, Using a Computational First-Principles Approach*, Phys. Rev. X **3**, 041035 (2013).

[10] C. Uher, J. Yang, S. Hu, D. T. Morelli, and G. P. Meisner, *Transport properties of pure and doped MNiSn (M=Zr, Hf)*, Phys. Rev. B **59**, 8615–8621 (1999).

[11] H. Hohl, A. P. Ramirez, C. Goldmann, G. Ernst, B. Wölfing, and E. Bucher, *Efficient dopants for ZrNiSn-based thermoelectric materials*, J. Phys.: Conden. Matt. **11**, 1697–1709 (1999).

[12] G. S. Nolas, J. Poon, and M. Kanatzidis, *Recent Developments in Bulk Thermoelectric Materials*, MRS Bull. **31**, 199–205 (2006).

[13] C. Yu, T.-J. Zhu, R.-Z. Shi, Y. Zhang, X.-B. Zhao, and J. He, *High-performance half-Heusler thermoelectric materials* $Hf_{1-x}Zr_xNiSn_{1-y}Sb_y$ *prepared by levitation melting and spark plasma sintering*, Acta Mater. **57**, 2757–2764 (2009).

[14] T. Sekimoto, K. Kurosaki, H. Muta, and S. Yamanaka, *Thermoelectric properties of (Ti,Zr,Hf)CoSb type half-Heusler compounds*, Mater. Trans., JIM **46**, 1481–1484 (2005).

[15] S. R. Culp, S. J. Poon, N. Hickman, T. M. Tritt, and J. Blumm, *Effect of substitutions on the thermoelectric figure of merit of half-Heusler phases at* 800°C, Appl. Phys. Lett. **88**, 042106 (2006).

[16] G. Joshi, X. Yan, H. Wang, W. Liu, G. Chen, and Z. F. Ren, *Enhancement in Thermoelectric figure of merit of an n-Type half-Heusler Compound by the Nanocomposite Approach*, Adv. Energy Mater. **1**, 643–647 (2011).

[17] X. Yan, G. Joshi, W. Liu, Y. Lan, H. Wang, S. Lee, J. W. Simonson, S. J. Poon, T. M. Tritt, G. Chen, and Z. F. Ren, *Enhanced Thermoelectric figure of merit of p-Type half-Heuslers*, Nano Lett. **11**, 556–560 (2011).

[18] X. Yan, W. Liu, H. Wang, S. Chen, J. Shiomi, K. Esfarjani, H. Wang, D. Wang, G. Chen, and Z. F. Ren, *Stronger phonon scattering by larger differences in atomic mass and size in p-type half-Heuslers* $Hf_{1-x}Ti_xCoSb_{0.8}Sn_{0.2}$, Energy Environ. Sci. **5**, 7543–7548 (2012).

[19] J. Shiomi, K. Esfarjani, and G. Chen, *Thermal conductivity of half-Heusler compounds from first-principles calculations*, Phys. Rev. B **84**, 104302 (2011).

[20] F. Casper, T. Graf, S. Chadov, B. Balke, and C. Felser, *Half-Heusler compounds: novel materials for energy and spintronic applications*, Semiconductor Science and Technology **27**, 063001 (2012).

[21] W. Xie, A. Weidenkaff, X. Tang, Q. Zhang, J. S. J. Poon, and T. M. Tritt, *Recent Advances in Nanostructured Thermoelectric half-Heusler Compounds*, Nanomaterials **2**, 379–412 (2012).

[22] S. Sakurada and N. Shutoh, *Effect of Ti substitution on the thermoelectric properties of (Zr,Hf)NiSn half-Heusler compounds*, Appl. Phys. Lett. **86**, 082105 (2005).

[23] J.-F. Li, W.-S. Liu, L.-D. Zhao, and M. Zhou, *High-performance nanostructured thermoelectric materials*, NPG Asia Mater. **2**, 152–158 (2010).

[24] S. Curtarolo, W. Setyawan, S. Wang, J. Xue, K. Yang, R. H. Taylor, L. J. Nelson, G. L. W. Hart, S. Sanvito, M. Buongiorno Nardelli, N. Mingo, and O. Levy, *AFLOWLIB.ORG: A distributed materials properties repository from high-throughput ab initio calculations*, Comp. Mat. Sci. **58**, 227–235 (2012).

[25] S. Curtarolo, W. Setyawan, G. L. W. Hart, M. Jahnatek, R. V. Chepulskii, R. H. Taylor, S. Wang, J. Xue, K. Yang, O. Levy, M. Mehl, H. T. Stokes, D. O. Demchenko, and D. Morgan, *AFLOW: an automatic framework for high-throughput materials discovery*, Comp. Mat. Sci. **58**, 218–226 (2012).

[26] X. Zhang, L. Yu, A. Zakutayev, and A. Zunger, *Sorting Stable versus Unstable Hypothetical Compounds: The Case of Multi-Functional ABX half-Heusler Filled Tetrahedral Structures*, Adv. Func. Mater. **22**, 1425–1435 (2012).

[27] F. Karlsruhe, *Inorganic Crystal Structure Database*, http://icsd.fiz-karlsruhe.de/icsd/.

[28] J. M. Ziman, *Electrons and Phonons: The Theory of Transport Phenomena in Solids* (Oxford University Press, 2001).

[29] A. Ward, D. A. Broido, D. A. Stewart, and G. Deinzer, *Ab initio theory of the lattice thermal conductivity in diamond*, Phys. Rev. B **80**, 125203 (2009).

[30] D. A. Broido, M. Malorny, G. Birner, N. Mingo, and D. A. Stewart, *Intrinsic lattice thermal conductivity of semiconductors from first principles*, Appl. Phys. Lett. **91**, 231922 (2007).

[31] W. Li, N. Mingo, L. Lindsay, D. A. Broido, D. A. Stewart, and N. A. Katcho, *Thermal conductivity of diamond nanowires from first principles*, Phys. Rev. B **85**, 195436 (2012).

[32] Y. Xia, S. Bhattacharya, V. Ponnambalam, A. L. Pope, S. J. Poon, and T. M. Tritt, *Thermoelectric properties of semimetallic (Zr, Hf)CoSb half-Heusler phases*, J. Appl. Phys. **88**, 1952–1955 (2000).

[33] T. Sekimoto, K. Kurosaki, H. Muta, and S. Yamanaka, *High-Thermoelectric Figure of Merit Realized in p-Type half-Heusler Compounds:* $ZrCoSn_xSb_{1-x}$, Jpn. J. Appl. Phys. **46**, L673–L675 (2007).

[34] P. Giannozzi, S. de Gironcoli, P. Pavone, and S. Baroni, *Ab initio calculation of phonon dispersions in semiconductors*, Phys. Rev. B **43**, 7231–7242 (1991).

[35] E. L. Lehmann, *Nonparametrics: Statistical Methods Based on Ranks* (Springer, New York, 2006).

[36] L. Breiman, *Random Forests*, Mach. Learn. **45**, 5–32 (2001).

[37] D. S. Palmer, N. M. O'Boyle, R. C. Glen, and J. B. O. Mitchell, *Random forest models to predict aqueous solubility*, J. Chem. Inf. Model. **47**, 150–158 (2007).

[38] L. Auret and C. Aldrich, *Unsupervised Process Fault Detection with Random Forests*, Ind. Eng. Chem. Res. **49**, 9184–9194 (2010).

[39] V. Svetnik, A. Liaw, C. Tong, J. C. Culberson, R. P. Sheridan, and B. P. Feuston, *Random forest: a classification and regression tool for compound classification and QSAR modeling*, J. Chem. Inf. Comput. Sci. **43**, 1947–1958 (2003).

[40] L. Pauling, *The Naturere of the Chemical Bond and the Structure of Molecules and Crystals: An Introduction to Modern Structural Chemistry* (Cornell University Press, New York, 1960), 3rd edn.

[41] D. G. Pettifor, *A chemical scale for crystal-structure maps*, Sol. State Commun. **51**, 31–34 (1984).

[42] S. P. Lloyd, *Least square quantization in PCM*, IEEE

Trans. Inf. Theory **28**, 129–137 (1982).

[43] G. A. Slack, *The thermal conductivity of nonmetallic crystals*, in *Solid State Physics*, edited by H. Ehrenreich, F. Seitz, and D. Turnbull (Academic, New York, 1979), vol. 34, p. 1.

[44] D. G. Cahill, S. K. Watson, and R. O. Pohl, *Lower limit to the thermal conductivity of disordered crystals*, Phys. Rev. B **46**, 6131–6140 (1992).

[45] D. T. Morelli, V. Jovovic, and J. P. Heremans, *Intrinsically Minimal Thermal Conductivity in Cubic I-V-VI_2 Semiconductors*, Phys. Rev. Lett. **101**, 035901 (2008).

[46] I. T. Jolliffe, *Principal component analysis* (Springer, New York, 2002).

[47] W. Setyawan and S. Curtarolo, *High-throughput electronic band structure calculations: challenges and tools*, Comp. Mat. Sci. **49**, 299–312 (2010).

[48] W. Setyawan, R. M. Gaume, S. Lam, R. S. Feigelson, and S. Curtarolo, *High-Throughput Combinatorial Database of Electronic Band Structures for Inorganic Scintillator Materials*, ACS Comb. Sci. **13**, 382–390 (2011).

[49] G. Kresse and J. Furthmüller, *Efficient iterative schemes for ab initio total-energy calculations using a plane-wave basis set*, Phys. Rev. B **54**, 11169–11186 (1996).

[50] P. E. Blöchl, *Projector augmented-wave method*, Phys. Rev. B **50**, 17953–17979 (1994).

[51] J. P. Perdew, K. Burke, and M. Ernzerhof, *Generalized gradient approximation made simple*, Phys. Rev. Lett. **77**, 3865–3868 (1996).

[52] H. J. Monkhorst and J. D. Pack, *Special points for Brillouin-zone integrations*, Phys. Rev. B **13**, 5188–5192 (1976).

[53] A. Togo, F. Oba, and I. Tanaka, *First-principles calculations of the ferroelastic transition between rutile-type and $CaCl_2$-type SiO_2 at high pressures*, Phys. Rev. B **78**, 134106 (2008).

[54] R Core Team, *R: A Language and Environment for Statistical Computing*, R Foundation for Statistical Computing, Vienna, Austria (2012).

[55] A. Liaw and M. Wiener, *Classification and Regression by randomForest*, R News **2**, 18–22 (2002).

[56] Y. Freund and R. E. Schapire, *A decision-theoretic generalization of on-line learning and an application to boosting*, J. Comput. Syst. Sci. **55**, 119–139 (1997).

[57] The decreasing trend can be understood considering that the specific heat per atom at high temperatures relates to the number of degrees of freedom, through the equipartition theorem. Hence a $c_v \propto a_{\mathrm{latt}}^3$ dependence should be expected. In fact, the observed trend is sharper, due to the differences in Debye temperature among the compounds.